Site survey : a new criterion for characterization of multipath environment

Eric Chatre, Frédéric Bastide, Christophe Macabiau

▶ **To cite this version:**

Eric Chatre, Frédéric Bastide, Christophe Macabiau. Site survey : a new criterion for characterization of multipath environment. ION NTM 2001, National Technical Meeting, Jan 2001, Long Beach, United States. pp 512-521. hal-01021703

HAL Id: hal-01021703
https://enac.hal.science/hal-01021703v1

Submitted on 30 Oct 2014

HAL is a multi-disciplinary open access archive for the deposit and dissemination of scientific research documents, whether they are published or not. The documents may come from teaching and research institutions in France or abroad, or from public or private research centers.

L'archive ouverte pluridisciplinaire **HAL**, est destinée au dépôt et à la diffusion de documents scientifiques de niveau recherche, publiés ou non, émanant des établissements d'enseignement et de recherche français ou étrangers, des laboratoires publics ou privés.

Site Survey: A New Criterion for Characterization of Multipath Environment

Eric CHATRE, *STNA*
Frédéric BASTIDE, *ENAC*
Christophe MACABIAU, *ENAC*

BIOGRAPHY

Eric Chatre graduated as an electronics engineer in 1992 from the ENAC (Ecole Nationale de l'Aviation Civile), Toulouse, France. Since 1994, he has been working with the Service Technique de la Navigation Aérienne (STNA) in Toulouse on implementation of satellite navigation in civil aviation. He is involved in the development of EGNOS and in the definition phase of Galileo. He is also participating in GNSS standardization activities in ICAO GNSSP and EUROCAE, RTCA forums.

Frederic Bastide will graduate in July 2001 as an electronics engineer from the Ecole Nationale de l'Aviation Civile (ENAC) in Toulouse, France. He intends to become a researcher in satellite radionavigation.

Christophe Macabiau is in charge of the signal processing unit of the CNS Research Laboratory (URE-CNS) at the Ecole Nationale de l'Aviation Civile (ENAC) in Toulouse, France. After working in 1993 for the MLS Project Office in Ottawa, Canada, he received his Ph.D. from the ENAC in 1997. He is currently working on the application of code and phase LADGPS positioning techniques to aeronautics.

ABSTRACT

The study reported in this paper is focused on the determination of a proper criterion for the characterization of the level of multipath affecting a particular station.

The paper starts with the description of new receiver structures allowing multiple correlator outputs inside a same tracking channel, and highlights the benefits of such designs. From the availability of this data, a new technique is proposed to quantify the deformations affecting the correlation peak. Two approaches are presented to solve this problem. One of them is based on a temporal criterion reflecting the noise variance affecting the correlation function. The second one is based on a spectral analysis and determines the unexpected spectral components in the correlation function. Specific algorithms are presented for the practical evaluation of these two metrics.

The paper describes the calibration of these criteria that is performed using a GPS RF signal generator delivering known multipath signals. Validation of the process was carried out through an extensive data collection campaign involving several sites and a number of antennas. Results with both methods enable to establish a consistent ranking of site/antenna pairs.

A further refinement of the techniques is considered using finer multipath identification based on observed and predicted multiple correlator outputs.

I. INTRODUCTION

The Ground Based Augmentation Systems aim at supporting very demanding applications such as CAT I, II and III precision approach operations. The achievable performance is highly dependent on the level of accuracy of the measurements made by the reference station, which is dominated by multipath.

The multipath errors affecting the pseudorange corrections transmitted by the reference station can be reduced in several ways, including careful siting, good antenna design, and adequate signal processing.

Several studies have focused on the analysis of multipath effects on receivers [Braasch 1996] and on the development of siting tools [Macabiau et al 2000], [Weiser, 1998], [Townsend et al 2000].

Effects of multipath on correlator outputs and discrimination functions are well known and briefly reviewed in part II. The purpose of the study is to quantify these effects for a particular site/antenna pair.

Multiple correlator structures enable to observe these effects more efficiently because they give access to the full correlation peak. As they are an important tool for the proposed quantification, these structure are presented in section III.

Through theoretical study and analysis of real data, two approaches were determined to quantify

multipath environment. These approaches are detailed in section IV.

Then, the two metrics are tested in various configurations and results are shown in section V.

In section 6, ways to improve the efficiency of the metrics are presented.

II. THEORETICAL ANALYSIS

The C/A signal entering the receiver tracking loops is the RF signal sensed by the antenna, fed to the RF unit where it is filtered, amplified, down-converted to intermediate frequency, sampled and quantized. The incoming composite C/A signal for one single satellite in presence of one diffracted signal and without noise is modeled as follows:

$$\begin{aligned} V(k) = & A_0(k)D(kT_s-\tau_0)C_f(kT_s-\tau_0)\cos(2\pi f_0 kT_s-\theta_0) \\ & +A_1(k)D(kT_s-\tau_1)C_f(kT_s-\tau_1)\cos(2\pi f_0 kT_s-\theta_1) \end{aligned} \quad (1)$$

where

- k is the discrete time index and T_s is the internal sampling period of the receiver.
- f_0 is the intermediate frequency of the receiver.
- A_0 and A_1 are respectively the amplitudes of the direct ray and the diffracted one.
- D is the P/NRZ/L waveform representing the navigation message.
- C_f is the P/NRZ/L waveform representing the C/A code as filtered by the RF unit.
- τ_i and θ_i are respectively the total group and phase propagation delays of the direct ray and the diffracted one. These quantities vary with time.

The operations performed by the tracking loops called the Phase Lock Loop (PLL) and the Delay Lock Loop (DLL) are illustrated in Figure 1 for a classical receiver. The aim of these tracking loops is to generate local replicas of the code and carrier that are synchronized with the line-of-sight signal. To achieve these objectives, the loops control local oscillators whose outputs are continuously compared with the incoming signal.

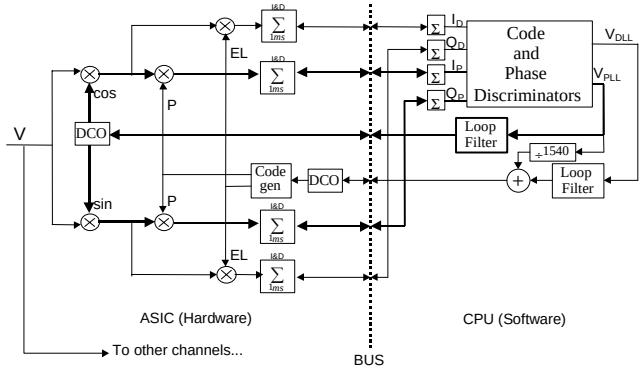

Figure 1 : *Architecture of a digital GPS receiver*

The input signal V is first down-converted into the I and Q channels by mixing it with the in-phase and quadrature outputs of the PLL local oscillator. Then, these two signals are multiplied by a punctual replica of the tracked C/A code, and M samples of the resulting signals are cumulated by the Integrate and Dump (I&D) filters to form the I_P and Q_P data that are later used to control the PLL and the DLL. In parallel, the initial I and Q channels are multiplied by a reference waveform denoted *EL* composed of a linear combination of code replicas with specific delays. This reference signal can have various expressions. For the Early minus Late DLL :

$$EL(k) = C(kT_s - \hat{\tau} - \frac{\Delta}{2}) - C(kT_s - \hat{\tau} + \frac{\Delta}{2}) \quad (2)$$

where Δ is the Early-Late chip spacing.

This product with the reference waveform EL(k) provides a combination of various correlation values called I_{DEL} and Q_{DEL} after integration by the I&D filters that are used to drive the DLL.

The I_P, Q_P, I_{DEL} and Q_{DEL} samples are then combined in a non linear fashion to form the PLL and DLL discrimination tensions V_{PLL} and V_{DLL}. These discrimination functions are finally filtered and fed to the PLL and DLL local oscillators.

For example, the discrimination function of the classical Early minus Late dot-product DLL is proportional to:

$$V_{DLL}(n) = \frac{I_{D_{EL}} I_P + Q_{D_{EL}} Q_P}{I_P^2 + Q_P^2} \quad (3)$$

the signals have the following expressions :

$$\begin{cases} I_{D_{EL}}(n) = \frac{A_0}{2} D(n) V(\varepsilon_{D_0}) \cos(\varepsilon_{P_0}) \\ \qquad\qquad + \frac{A_1}{2} D(n) V(\varepsilon_{D_1}) \cos(\varepsilon_{P_1}) \\ Q_{D_{EL}}(n) = \frac{A_0}{2} D(n) V(\varepsilon_{D_0}) \sin(\varepsilon_{P_0}) \\ \qquad\qquad + \frac{A_1}{2} D(n) V(\varepsilon_{D_1}) \sin(\varepsilon_{P_1}) \end{cases} \quad (4)$$

where

- n is the index of the time series delivered by the I&D filter.
- $\varepsilon_{D_i} = \tau_i - \hat{\tau}$ is the deviation between the group delay of ray i and the code delay estimate.
- $\varepsilon_{P_i} = \theta_i - \hat{\theta}$ is the deviation between the phase propagation delay of the ray i and the carrier phase delay estimate.
- D is the navigation message.
- $V(\varepsilon) = R(\varepsilon + \frac{\Delta}{2}) - R(\varepsilon - \frac{\Delta}{2})$
- R is the cross-correlation function of the incoming filtered code and the locally generated code, as presented in (5):

$$R(\varepsilon) = \sum_{m=0}^{M-1} C((k-m)T_s - \hat{\tau}) C_f((k-m)T_s - \tau) \quad (5)$$

Moreover,

$$\begin{cases} I_P(n) = \frac{A_0}{2} D(n) R(\varepsilon_{D_0}) \cos(\varepsilon_{P_0}) \\ \qquad + \frac{A_1}{2} D(n) R(\varepsilon_{D_1}) \cos(\varepsilon_{P_1}) \\ Q_P(n) = \frac{A_0}{2} D(n) R(\varepsilon_{D_0}) \sin(\varepsilon_{P_0}) \\ \qquad + \frac{A_1}{2} D(n) R(\varepsilon_{D_1}) \sin(\varepsilon_{P_1}) \end{cases} \quad (6)$$

When the reference signal *EL(k)* is a simple Early minus Late function as in (2), and when the incoming signal is the signal modeled as in (1), it can be shown that the discrimination function has the expression (7) given below:

$$\begin{aligned} V_{DLL}(n,\Delta) = & A_0{}^2 V(\varepsilon_{D_0}) R(\varepsilon_{D_0}) \\ & + A_1{}^2 V(\varepsilon_{D_1}) R(\varepsilon_{D_1}) \\ & + A_0 A_1 \cos(\Delta\theta) \left[V(\varepsilon_{D_0}) R(\varepsilon_{D_1}) + V(\varepsilon_{D_1}) R(\varepsilon_{D_0}) \right] \end{aligned} \quad (7)$$

where $\Delta\theta = \theta_1 - \theta_0$ is the deviation between the phase propagation delay of the diffracted ray and the direct one.

Concerning the PLL, a classical discrimination function is given by :

$$V_{PLL} = \arctan\left(\frac{Q_P(n)}{I_P(n)} \right) \quad (8)$$

where the expressions of Q_P and I_P are given by (6).

As we can see in (7) and (8), the discrimination functions V_{DLL} and V_{PLL} are distorted because the correlator outputs are affected by multipath. These distortions induce non zero steady-state tracking errors ε_{D_0} and ε_{P_0}. Therefore, the analysis of the correlator outputs is one of the main element for the determination of the effect of multipath on the tracking error.

III. MULTICORRELATOR TECHNOLOGY

Classical receivers offer several tracking channels, each of them being driven by two pairs of correlator outputs. A new receiver structure allows multiple correlator outputs for each tracking channel. For this study, we have used a Novatel receiver in a configuration where it tracks one satellite and provides 48 correlation outputs inside that channel. As a consequence, 48 measurements on the correlation peak (I channel) are available ranging from about –1 chip to 1.4 chip w.r.t. punctual. Similarly, 48 measurments are available for the Q channel.

The basic structure of one correlator is illustrated in Figure 2.

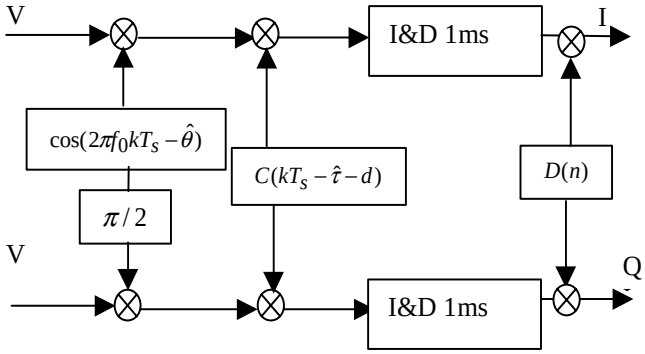

Figure 2 : Structure of a generic correlator output

where

- *V* is the incoming signal given in (1).
- $\hat{\tau}$ and $\hat{\theta}$ are provided respectively by the DLL and the PLL.
- *d* is the offset with respect to the punctual

Expressions of the signal on the I and Q channels for a given correlator offset *d* are :

$$\begin{cases} I(n) = \frac{A_0}{2} R(\varepsilon_{D_0} - d) \cos\varepsilon_{P_0} + \frac{A_1}{2} R(\varepsilon_{D_1} - d) \cos\varepsilon_{P_1} \\ Q(n) = \frac{A_0}{2} R(\varepsilon_{D_0} - d) \sin\varepsilon_{P_0} + \frac{A_1}{2} R(\varepsilon_{D_1} - d) \sin\varepsilon_{P_1} \end{cases}$$

We carried out a simulation campaign so as to highlight the efficiency of such structures to show effects of multipath on the correlation peak. Using a GPS RF signal generator, we simulated a direct ray plus one diffracted ray whose relative delay with respect to the direct signal can be changed. Moreover, for each particular value of the delay, the phase of the carrier is continuously rotated over an interval of 3 wavelengths. This is done to explore the full envelope of the correlation peak. The relative amplitude of the reflected ray is set to 0.25. Figure 3 to Figure 5 present observed results for several values of relative delays.

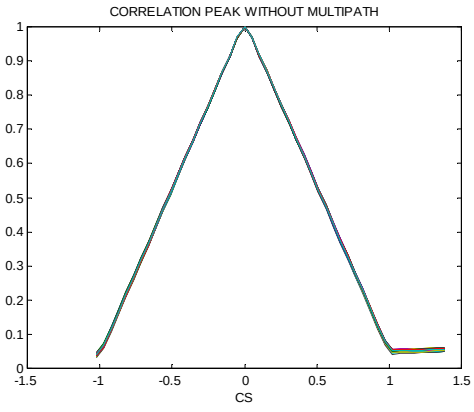

Figure 3 : Observed correlation peak without multipath

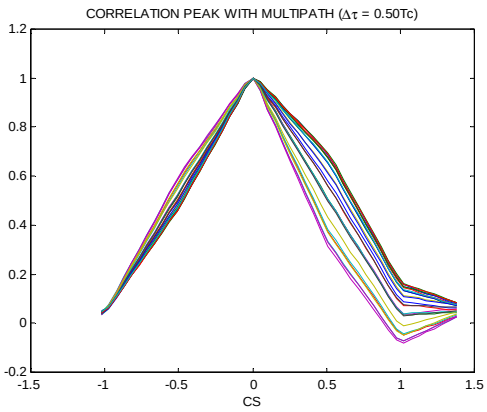

Figure 4 : Observed correlation peak with a 0.5 chip relative delay

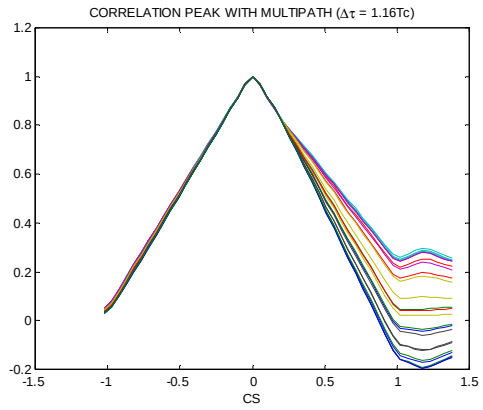

Figure 5 : Observed correlation peak with a 1.16 chip relative delay

We can see, that these observed correlation samples are consistent with the classical in-phase/out-of-phase construction of correlation peaks. As expected, the more the relative delay increases the more the positive side of the correlation peak is affected.

IV. PROPOSED METRICS

Considering the theroretical results presented in the previous section, two separate options were considered to characterize the multipath environment.

Time Domain Method

The first method analyzed, relies on the fact that distortions of the correlation peak induced by multipath are variable in time. and reflect the induced tracking errors. A metric characterizing the fluctuations of each correlator output is therefore likely to inform on the quality of the environment. Figure 6 presents all correlator outputs (I channel) for a given satellite over a period of time in a typical environment.

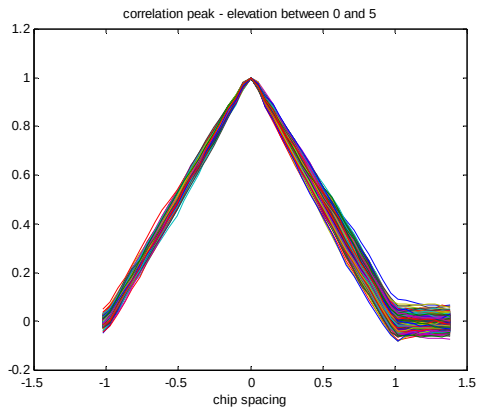

Figure 6: Correlation peak over time for a satellite at low elevation angle

The ideal correlation peak is subtracted from the measurements in order to extract residual errors. Data is then sorted in 5° elevation bins and the standard deviation of each residual correlator output is computed. This provides 48 values representing the noise affecting the correlation peak for each delay wrt punctual as shown in Figure 7 and Figure 8 for satellite at low and high elevation angles.

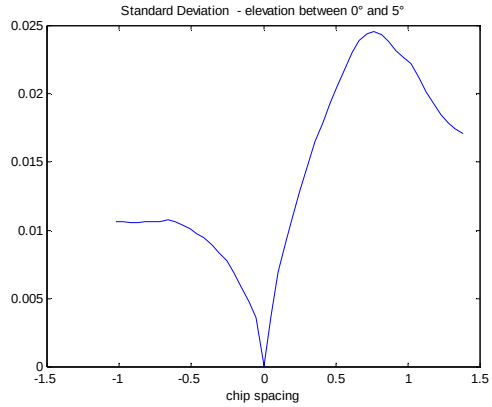

Figure 7 : Standard deviations of correlator outputs for low elevation satellite

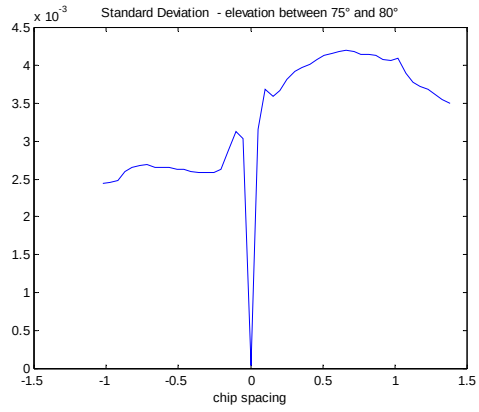

Figure 8 : Standard deviations of correlator outputs for high elevation satellite

As expected, the noise affecting the correlation peak is significantly lower for high elevation satellite. Additionally, the asymmetry between the leading and falling edges of the correlation peak is significantly magnified when considering low elevation satellites. This is because multipath mainly affects the positive side of the correlation peak.

In order to take credit of this lopsidedness, the final metric is computed as follows :

$$M_{STD}(\theta) = \left| \sum_{k>0} \sigma_{CS}^2(k) - \sum_{k<0} \sigma_{CS}^2(k) \right|_{\theta \in bin}$$

To test the metric, data was collected using a GPS signal generator in presence of multipath. Different scenarios were run corresponding to various multipath amplitudes and relative delays. Results are provided in ***Table 1*** and ***Figure 9*** below.

Delay (Chip) / Attenuation	0.2	0.4	0.6	0.8	1	1.1	1.15
12 dB	0.59	1.39	1.95	2.39	2.52	2.48	2.23
6 dB	1.28	2.98	4.00	4.73	5.15	5.09	4.41
3 dB	1.86	4.41	5.69	6.69	7.21	6.93	6.20

Table 1 : Results of calibration for M_{STD}

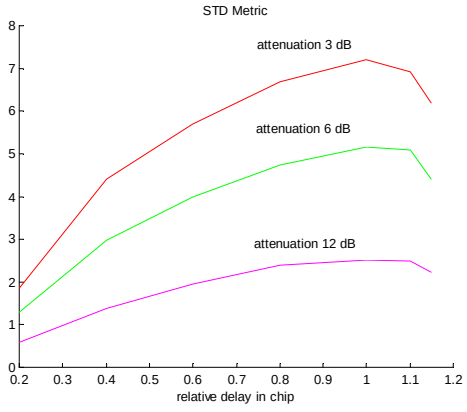

Figure 9 : Results of calibration for M_{STD}

The calibration results confirm that the metric has the expected evolution with respect to the multipath amplitude & delay. Metric values increase for high multipath amplitude and for large multipath delays.

Frequency Domain Method

The second method investigated relies on the low frequency distortion introduced by multipath on the correlation peak at any given time. It is therefore necessary to extract the multipath from the measured correlation peak.

The nominal correlation peak accounting for the receiver RF front end can be measured using data collected with a GPS signal generator and is subtracted from the measured correlator outputs as illustrated in ***Figure 10*** .

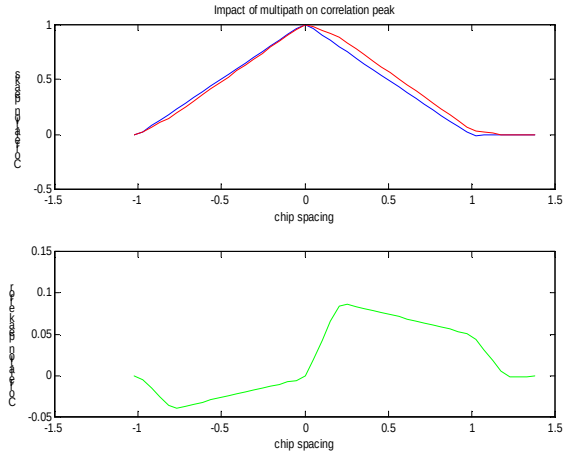

Figure 10 : Low frequency component introduced by multipath of correlation peak error

The second type of metric studied consists in computing the Fast Fourier Transform of the correlation peak residual errors for each time sample and averaging these over a satellite elevation bin. It is anticipated that the continuous component of this quantity (averaged FFT evaluated for null frequency) gives a good idea of the multipath environment. The corresponding metric can be defined as :

$$M_{FFT}(\theta) = \frac{1}{n} \sum_{\theta \in bin} \left| FFT(Peak_{measured} - Peak_{calib}) \right|_{f=0}$$

Figure 7 illustrates the different steps described above for a low elevation satellite.

In fact, it is necessary to further process the raw measurements so as to compensate the effect of lead/lag constantly generated by the receiver tracking loop and that introduces a spurious low frequency component in the FFT metric. The disturbance of this lead/lag phenomenon effects symmetrically each correlator pair. For a lead, the Early sample is biased positively while the Late sample is biased negatively by the same amount. The unwanted effect in therefore eliminated by folding the leading edge of the correlation peak over the falling edge prior to FFT computation. This explains why FFTs presented in the paper consist in only 21 samples while 41 correlation peak measurements (between ±1 chip) were initially available.

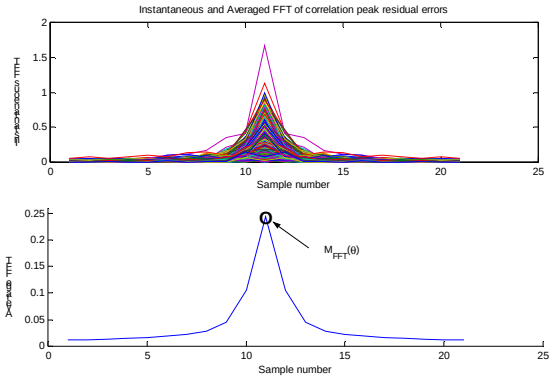

Figure 11 : Instantaneous and Averaged FFT for low elevation satellite

Similarly to what was done for the first metric, a test campaign was conducted using a signal generator to check the validity of the concept. Testing conditions and corresponding results are provided in ***Table 2*** and ***Figure 12***.

Delay (Chip) / Attenuation	0.2	0.4	0.6	0.8	1	1.1	1.15
12 dB	1.69	1.27	1.42	2.28	2.00	1.35	1.49
6 dB	1.96	2.32	2.83	2.85	3.61	2.57	2.37
3 dB	2.49	3.33	3.93	4.97	4.76	3.57	3.23

Table 2 : Results of calibration for M_{FFT}

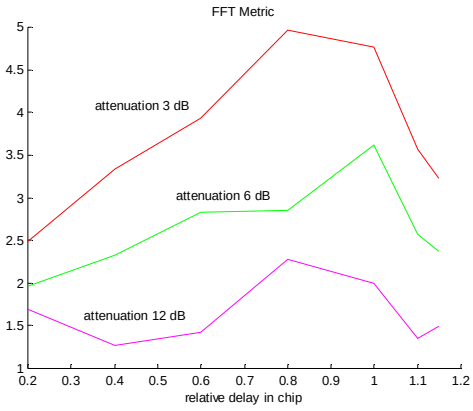

Figure 12 : Results of calibration for M_{FFT}

Again, results show that the metric globally reflects the seriousness of the multipath environment. However, the results are not as well behaved as the ones gotten with the STD metric.

V. RESULTS OF DATA COLLECTION

The next step was to check the behavior of the two metrics described above in different test configurations. Two key parameters with regards to multipath disturbances have been tested : 1) site location and 2) antenna design.

Data was collected at three sites :

- Site 1 - Roof of STNA Building : No specific siting criteria adopted to choose the site. A priori multipath environment is Medium. Two separate antenna locations were investigated.
- Site 2 - Roof of ENAC building : No specific siting criteria adopted to choose the site. A priori multipath environment is Medium.
- Site 3 - GBAS ground reference station in Blagnac Airport : Obstacle free environment chosen during GBAS site survey.

The data was collected using different antennas as follows:

- Novatel 502. No choke ring is used in this basic configuration.
- NovAtel 501 : a high performance, active antenna which provides a superior low elevation angle gain. The 501 also provides enhanced multipath rejection. A choke ring is added that can reduce code and carrier phase multipath by up to 50 per cent
- Novatel 503 designed to operate at the GPS L1 and L2 frequencies. It incorporates a choke ring which substantially reduces the multipath effects on the GPS signal by reducing the antenna gain at low elevation.

For each Site/Antenna pair, all correlator outputs data were recorded for at least one full pass of PRN 1. PRN 1 has a long visibility interval and spans all elevation angles up to around 85° in Toulouse.

Results of STD metric

Figure 13 to Figure 15 present test results for the three sites studied.

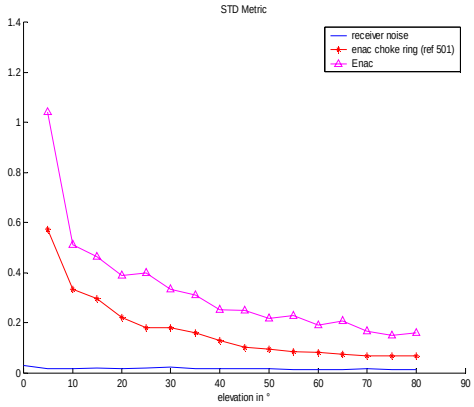

Figure 13 : Test results for STD metric at ENAC

For each case, the lower curve corresponds to the metric computed for a signal not affected by multipath. This calibration was obtained using a signal generator.

It is interesting to notice that results are very repeatable over time. Three passes of PRN 1 were recorded in STNA over one week and give almost identical results. The same conclusion is reached for data collected in ENAC which indicates that the chosen metric is stable and not sensitive to minor transient effects.

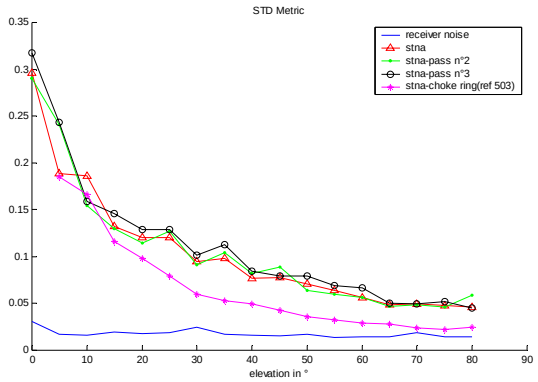

Figure 14 : Results of STD metric at STNA

For both sites 1 and 2, results show that the use of choke ring antennas noticeably reduces the observed metric values. This is consistent with the expected reduction of multipath effect introduced by such devices.

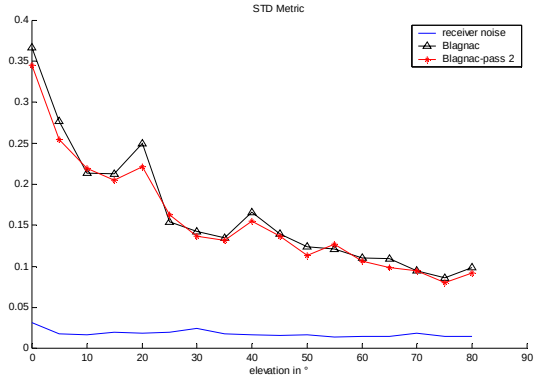

Figure 15 : Results of STD metric at Blagnac

In order to establish a ranking of each of the Site/Antenna pair studied, an overall metric is computed covering all elevation angles between 5 and 85°.

$$OM_{STD} = \sum_{5 \le \theta < 80} \left(M^2_{STD}(\theta) - M^2_{STDCal}(\theta) \right)$$

The final results are presented in ***Table 3***

	Enac	Enac-choke ring	Stna-ant3	Stna-ant3-choke ring	Stna-ant2	Stna-ant2-choke ring	Blag nac
STD Metric	1.57	0.86	0.42	0.32	0.68	0.20 (*)	0.63
Ranking	7th	6th	3rd	2nd	5th	1st	4th

Table 3 : Results for STD Overall metric

(*) The overall metric could only be computed over the 10°-85° elevation range. However, given the shape of the curve, it is anticipated that it corresponds to the best pair.

Results of FFT metric

Figure 16 to Figure 18 present test results for the three sites studied using the FFT metric. Again, the lower curve represents results obtained during the calibration run.

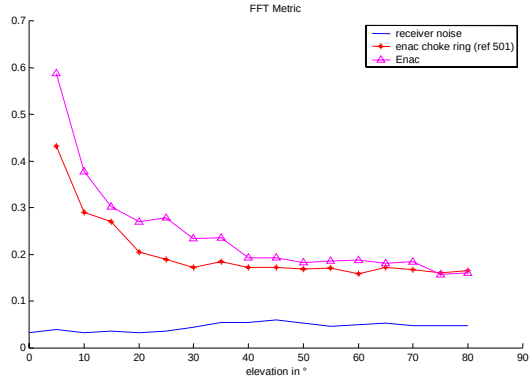

Figure 16 : Test results for FTT metric at ENAC

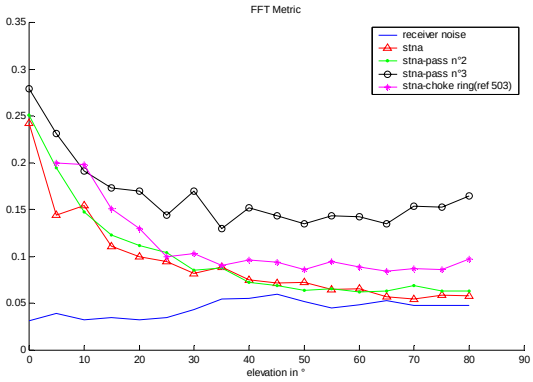

Figure 17 : Test results for FTT metric at STNA

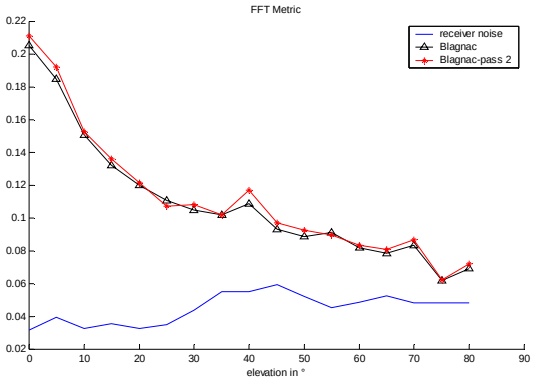

Figure 18 : Test results for FTT metric at Blagnac

Similarly to previous results, the FFT metric seems to reflect correctly the multipath environment. Results are globally repeatable even though there is a clear singularity in one of the three passes for site 2. At this point in time, this deviation is not explained but it is not only an outlier problem since the results show significant differences for all elevation angles. This anomaly will be analysed further since persistence of such phenomenon would discredit the technical solution. Additionally, for data collected at site 2, the FFT metric does not show any improvement when using a choke ring antenna. This is contradictory to both STD metric results and engineering

judgement. More data will be collected to investigate further these findings.

An overall metric was also computed for all sites studied in order to compare their characteristics.

$$OM_{FFT} = \sum_{5\le\theta\le80}\left(M_{FFT}(\theta) - M_{FFT\ cal}(\theta)\right)$$

Final results are presented in ***Table 4***

	Enac	Enac-choke ring	Stna-ant3	Stna-ant3-choke ring	Stna-ant2	Stna-ant2-choke ring	Blagnac
FFT Metric	3.18	2.52	1.05	1.06	2.08	0.81	0.95
Ranking	5th	4th	(**)	2nd	3rd	(*)	1st

Table 4 : Results for FFT overall metric

(*) The overall metric could only be computed over the 10°-85° elevation range. Unlike with the STD case, it was not possible to extrapolate the results to rank this site.
(**) Since one of the satellite pass was significantly off, we decided not to rank this site.

Final comparison

	Enac	Enac-choke ring	Stna-ant3	Stna-ant3-choke ring	Stna-ant2	Stna-ant2-choke ring	Blagnac
STD Metric	5th	4th		1st	3rd		2nd
FFT Metric	5th	4th		2nd	3rd		1st

Table 5 : Comparison of both overall metrics

When comparing results over Site/Antenna pairs for which there is a good confidence on the data and the metric processing, Table 5 shows very good consistency of both methods.

Unexpectedly, STNA roof site gets a good ranking tied with Blagnac GBAS shelter site. ENAC roof site is definitely perturbed by more serious multipath.

VI. FORESEEN IMPROVEMENTS

The principle of the metric can be improved by using only 12 correlator outputs inside a same channel. It enables us to track 4 satellites at once.

We have to find parts of the correlation peak that could show the influence of multipaths efficiently. Only improvements of the STD metric have been studied and the new metric uses the last 6 points on the correlation peak's leading edge ant the first 6 points on the falling edge. This new metric is computed as follows :

$$M_{STD}(\theta) = \left| \sum_{k>0}^{6} \sigma^2_{CS}(k) - \sum_{k=-6}^{-1} \sigma^2_{CS}(k) \right|_{\theta \in bin}$$

In order to test the behavior of the new metric, recordings described in part IV were used. Figure 21 to Figure 23 present test results for the three sites studied.

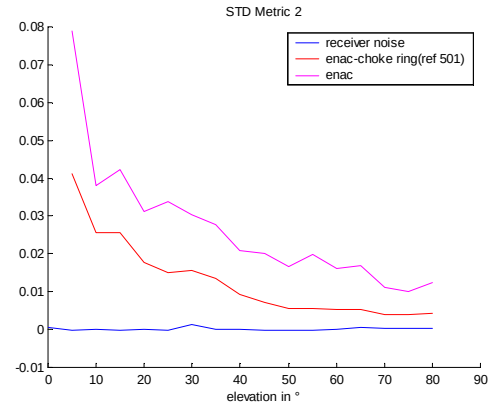

Figure 19 : Test results for new STD metric at ENAC

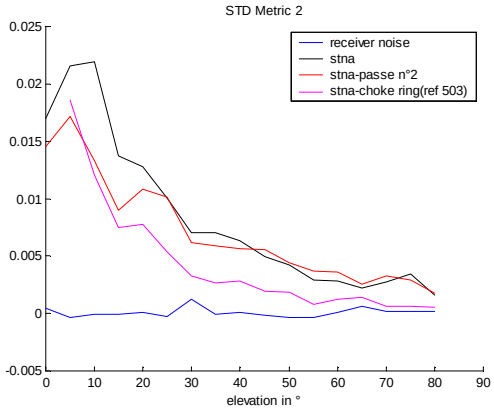

Figure 20 : Test results for new STD metric at STNA

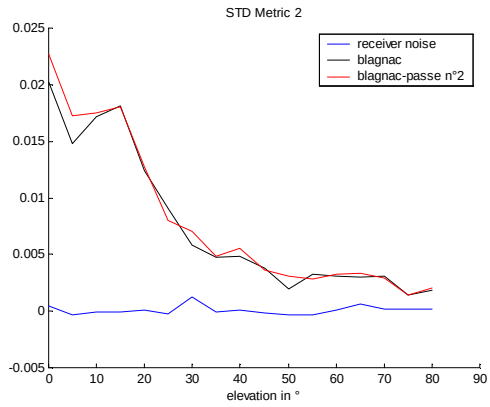

Figure 21 : Test results for new STD metric at Blagnac

Improvements of the FFT metric will be investigated later.

VII CONCLUSION

The objective of our study was to develop a metric able to characterize accurately the effect of multipath on a ground reference receiver. Based on theoretical analysis and using measurements available from a multicorrelator receiver, two different metrics in both time and frequency domains were created likely to be representative of multipath environment.

Test results confirmed that both metrics were reliable and could be used to establish a hierarchy between site/antenna pairs during a site survey campaign. However, it was shown that the STD metric produces more repeatable results than the FFT metric. For this reason, further development of the work will be carried out using the STD metric which seems more robust.

The current study is based on analysis of only one satellite at a time and uses 40 correlator readings throughout the correlation peak. This is clearly sub-optimal since the multipath environment can be well characterized using a more limited set of carefully chosen correlator readings. Initial results based on 12 correlator outputs are encouraging since they duplicate the results obtained with the full set of measurements. Further analysis will be conducted in the near future to reduce even more the input data in order to increase the number of satellites analyzed simultaneously.

Finally, correlation between the metric values and receiver pseudorange tracking errors will be performed in order to fully validate the concept.

ACKNOWLEDGMENTS

This study was made possible through the joint funding of STNA and the European Commission in the frame of TEN/99/179 project for Pre-Operational Data Gathering to Support Multi-Modal SBAS Certification.

REFERENCES

[Bastide et Julien, 2000] F. BASTIDE and O. JULIEN « Effects of Interference and Multipath on GPS signals »,

[Bastide 2000] F. BASTIDE, « Study of Metrics characterizing Multipath Environment »

[Braasch 1996] M. BRAASCH “Global position system : Theory and applications” Volume 1, Chapter ‘Multipath Effects’, AIAA.

[Macabiau et al 2000], C. MACABIAU, B. ROTURIER, E. CHATRE, A.RENARD “GPS reference station siting tool”, Proceedings of ION NTM 2000.

[Weiser, 1998], M. WEISER “Influence of GNSS ground station siting on multipath errors”, WP 16, ICAO GNSSP WG B meeting, Wellington

[Townsend et al 2000], B. TOWNSEND, J. WIEBE, A. JAKAB “Results and Analysis of using the MEDDL receiver as a multipath meter. Proceedings of ION NTM 2000.